Testing and modeling a scroll expander integrated into an organic rankine cycle

Vincent Lemort, Sylvain Quoilin, Cristian Cuevas, Jean Lebrun

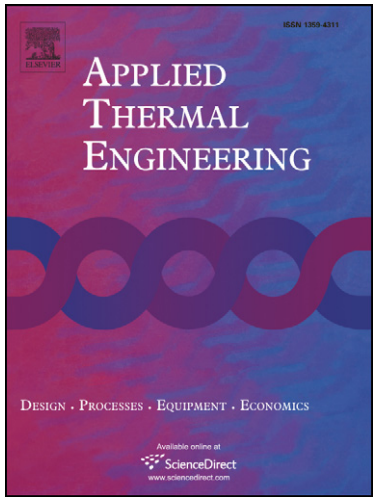

Testing and modeling a scroll expander integrated into an organic rankine cycle

Vincent Lemort, Sylvain Quoilin, Cristian Cuevas, Jean Lebrun

PII: S1359-4311(09)00117-3
DOI: 10.1016/j.applthermaleng.2009.04.013
Reference: ATE 2776

To appear in: *Applied Thermal Engineering*

Received Date: 25 July 2008
Accepted Date: 1 April 2009

Please cite this article as: V. Lemort, S. Quoilin, C. Cuevas, J. Lebrun, Testing and modeling a scroll expander integrated into an organic rankine cycle, *Applied Thermal Engineering* (2009), doi: 10.1016/j.applthermaleng.2009.04.013

TESTING AND MODELING A SCROLL EXPANDER INTEGRATED INTO AN ORGANIC RANKINE CYCLE

Vincent LEMORT*
Laboratoire de Thermodynamique, Université de Liège
Campus du Sart Tilman – Bâtiment B49, Parking P33
B-4000 Liège - Belgium
Phone: 32-4-3664824, Fax: 32-4-3664812
e-mail: vincent.lemort@ulg.ac.be
*Corresponding author

Sylvain QUOILIN
Laboratoire de Thermodynamique, Université de Liège
Campus du Sart Tilman – Bâtiment B49, Parking P33
B-4000 Liège - Belgium
Phone: 32-4-3664822, Fax: 32-4-3664812
e-mail: squoilin@ulg.ac.be

Cristian CUEVAS
Departamento de Ingeniería Mecánica, Facultad de Ingeniería
Universidad de Concepción
Casilla 160-C, Concepción
Chile
Phone: 56-41-2203550, Fax: 56-41-2251142
e-mail: crcuevas@udec.cl

Jean LEBRUN
Laboratoire de Thermodynamique, Université de Liège
Campus du Sart Tilman – Bâtiment B49, Parking P33
B-4000 Liège - Belgium
Phone: 32-4-3664801, Fax: 32-4-3664812
e-mail: j.lebrun@ulg.ac.be

ABSTRACT

Organic Rankine Cycles (ORC's) are particularly suitable for recovering energy from low-grade heat sources. This paper first presents the results of an experimental study carried out on a prototype of an open-drive oil-free scroll expander integrated into an ORC working with refrigerant HCFC-123. By exploiting the overall expander performance measurements, the eight parameters of a scroll expander semi-empirical model are then identified. The model is able to compute variables of first importance such as the mass flow rate, the delivered shaft power and the discharge temperature, and secondary variables such as the supply heating-up, the exhaust cooling-down, the ambient losses, the internal leakage and the mechanical losses. The maximum deviation between the predictions by the model and the measurements is 2% for the mass flow rate, 5% for the shaft power and 3K for the discharge temperature. The validated model of the expander is finally used to quantify the different losses and to indicate how the design of the expander might be altered to achieve better performances. This analysis pointed out that the internal leakages and, to a lesser extent, the supply pressure drop and the mechanical losses are the main losses affecting the performance of the expander.

Keywords:

Scroll, expander, Rankine cycle, heat recovery

NOMENCLATURE

A	area, m^2
AU	heat transfer coefficient, W/K
c	specific heat, J/kg-K
h	specific enthalpy, J/kg
$\dot{M}$	mass flow rate, kg/s
N	rotational speed [s^{-1}]
P	pressure, Pa
$\dot{Q}$	heat transfer rate, W
r	ratio, -
s	specific entropy, J/kg-K
t	temperature, C
T	torque, N.m
u	specific internal energy, J/kg
v	specific volume, m^3/kg
$\dot{V}$	volume flow rate, m^3/s
w	specific work, J/kg
$\dot{W}$	power, W

Greek letters

Δ	difference, -

ε	effectiveness, -
φ	filling factor, -
γ	isentropic exponent,-

Subscripts

ad	adapted
amb	ambient
calc	calculated
cp	compressor
crit	critical
dis	discharge
ex	exhaust
exp	expander
expan	expansion
in	internal
leak	leakage
loss	mechanical loss
meas	measured
n	nominal
p	constant pressure
s	isentropic or “swept”
sh	shaft
su	supply

suc	suction
thr	throat
tqm	torque-meter
v	volumetric
w	envelope

1. INTRODUCTION

Due to environmental constraints, the interest in low grade heat recovery has grown dramatically in the past decades. An important number of new solutions have been proposed to generate electricity from low temperature heat sources and are now applied to very diverse fields such as solar thermal power, geothermal heat sources, engine exhaust gases, domestic boilers, etc.

Among the solutions currently proposed, the Organic Rankine Cycle (ORC) is the most widely used. Its main advantages are its simplicity and its commonly available components. In such a cycle, the working fluid is an organic product that presents a lower ebullition temperature than water, allowing reduced evaporating temperatures.

Unlike traditional power cycles, local and small-scale energy production is made possible with this technology (Kane [1], Quoilin [2]).

The expander is a key element of the ORC. The choice of the expander strongly depends on the operating conditions and on the size of the facility. Two main types of machines can be distinguished: the dynamic (turbo) and displacement (volumetric) type. Displacement type machines are more appropriate to the small-scale ORC unit under investigation in this paper, because they are characterized by lower flow rates, higher pressure ratios and much lower rotational speeds than turbo-machines (Persson [3]). Moreover, these machines can tolerate two-phase conditions, which may appear at the end of the expansion in some operating conditions.

Among positive displacement machines, the scroll machine is a good candidate for the ORC application, because of its reduced number of moving parts, reliability, wide output power range, and broad availability (Zanelli and Favrat [4]). Moreover, it is a proven technology in compressor mode due to its extensive use in refrigeration and air-conditioning industry.

However, up to now, the use of scroll machines in expander mode has mainly been limited to experimental work and so far numerous scroll expander prototypes have been tested for different fluids.

For instance, Yanagisawa et al. [5] carried out an experimental study on an oil-free scroll-type air expander. They observed that the performance is heavily reduced by the mechanical loss, but leakage loss becomes significant as the rotational speed decreases. Maximal achieved volumetric and isentropic effectiveness was respectively 76% and 60%. Zanelli and Favrat [4] carried out an experimental investigation on a hermetic

scroll expander-generator fed with refrigerant R134a. The machine produced a power ranging from 1.0 to 3.5 kW with a maximal isentropic effectiveness of 65%. Kane [1] designed, built and tested a prototype of hybrid solar thermal power plant associating solar collectors, cogeneration engines and two superposed Organic Rankine Cycles, equipped with hermetic scroll expanders. Manzagol et al. [6] studied a cryogenic scroll expander used for a 10 L/h helium liquefier. The expander was tested on a Brayton cycle refrigerator and reached an isentropic effectiveness of 50 to 60% for supply gas conditions of 35 K and 0.7 MPa. Xiaojun et al. [7] investigated the possibility to recover work in a fuel cell by means of a scroll expander. The work produced by the expander could be provided to the compressor. Hugenroth et al. [8] developed a novel approach to implementing a gas Ericsson cycle heat pump, using liquid flooding of the compressor and of the expander to approach isothermal compression and expansion process. Scroll machines were selected due to their ability to compress and expand a mixture of oil and gas. Aoun and Clodic [9] investigated the same expander as Yanagisawa et al. [5], but operating with steam. In order to improve the volumetric performance, original tip seals were replaced by PTFE tip seals, better adapted for high temperature applications and presenting lubricating properties. Maximal achieved volumetric and isentropic effectiveness was respectively 63% and 48%.

This paper presents a semi-empirical simulation model of a scroll expander. Unlike deterministic models (that require the exact knowledge of the geometry of the machine), the model proposed only involves a limited number of parameters. By using experimental data these parameters will be identified in the case of a prototype of an expander fed with HCFC-123.

2. EXPERIMENTAL INVESTIGATION

2.1. Description of the test rig

An experimental investigation is carried out on a scroll expander integrated into a prototype of an ORC system working with refrigerant HCFC-123. This paper only focuses on the experimental characterization of the scroll expander and not of the entire ORC system.

The test rig is schematically described in Figure 1. The expander is originally an open-drive oil-free air scroll compressor. The only modifications made to the original compressor were to remove the cooling fan and to insulate the machine. The scroll expander has a kinematically rigid configuration, which maintains a small clearance gap between the scroll flanks (Peterson et al. [10]). Moving tip seals are embedded in a groove at the tip of both scrolls to reduce radial leakages (Inaba et al. [11]).

The expander drives an asynchronous machine through two belt-and-pulley couplings and a torque-meter. Using an asynchronous machine is a convenient way to impose the rotational speed of the expander. The boiler of the cycle is made up of three plate heat exchangers HX1, HX2 and HX3 in series, fed with hot air. The condenser is made up of two plate heat exchangers in parallel and is fed with chilled water. A diaphragm pump drives the refrigerant through the cycle. Its displacement can be adjusted, which allows controlling the refrigerant flow rate through the cycle.

The expander mechanical power is determined by measuring simultaneously the rotational speed and the torque developed at the torque-meter shaft. The transmission belt efficiency is estimated. The refrigerant flow rate is measured by a Coriolis flow meter located downstream of the pump. Temperatures are measured by means of T-type thermocouples (copper-constantan) and pressures are measured with piezoresistive pressure transmitters. The accuracy of the measurements involved in the evaluation of the expander performance is given in Table 1.

2.2. Description of the tests

The experimental data covers a large range of operating conditions. In total, 39 points are achieved. Table 2 indicates what are the imposed and the obtained variables during the tests. The refrigerant flow rate flowing through the expander is imposed by varying the pump displacement. The expander supply temperature is controlled by modifying the air flow rates and temperatures in the boiler. The expander rotational speed is set to 3 different values (1771, 2296, 2660 rpm) by modifying the diameter of the pulley at the asynchronous machine shaft. The expander exhaust pressure is imposed by adjusting the water flow rate through the condenser. Table 2 indicates that the vapor is superheated at the expander supply for all of the performance points.

2.3. Results

The ranges of the main measured variables are given in Table 2. The maximum delivered shaft power is 1.82 kW and the maximum achieved overall isentropic

effectiveness is 68%. This overall effectiveness is defined by the ratio of the measured shaft power and the isentropic power (Eq. (1)). The latter is the product of the measured flow rate by the expansion work associated to an isentropic expansion from supply conditions to the exhaust pressure:

$$\varepsilon_{s,meas} = \frac{\dot{W}_{sh,meas}}{\dot{W}_s} = \frac{\dot{W}_{sh,meas}}{\dot{M}_{meas}.w_s} = \frac{\dot{W}_{sh,meas}}{\dot{M}_{meas}.(h_{su} - h_{ex,s})} \quad (1)$$

The evolution of the overall isentropic effectiveness with the pressure ratio imposed to the expander for the three rotational speeds is given in Figure 2. The sharp decrease in effectiveness for the low pressure ratios is due to over-expansion losses. Error bars are associated with calculated uncertainties. Provided measurements are uncorrelated and random, the uncertainty U_Y on the variable Y is calculated as function of the uncertainties U_{Xi} on each measured variables X_i by Eq. (2) (Klein [12]).

$$U_Y = \sqrt{\sum_i \left(\frac{\partial Y}{\partial X_i}\right)^2 U_{X_i}^2} \quad (2)$$

Figure 2 also shows that the maximum achieved pressure ratio is around 5.5. Further experimental work should allow evaluating the performance of the expander for higher pressure ratios.

The volumetric performance of the expander is represented by the filling factor (Zanelli and Favrat [4]). The latter is defined as the ratio between the measured mass flow rate

and the mass flow rate theoretically displaced by the expander (Eq. (3)). The filling factor increases with internal leakage and supply cooling down, but decreases with the supply pressure drop.

$$\phi_{meas} = \frac{\dot{M}_{meas}.v_{su}}{\dot{V}_s} \quad (3)$$

The evolution of the filling factor with the expander supply pressure for the three rotational speeds is given in Figure 3. The filling factor could be expected to increase with the supply pressure due to larger internal leakage flows. However, this trend is balanced by the simultaneous effect of the supply pressure drop. It can be observed that the lower the rotational speed, the higher the filling factor, due to the larger relative impact of the internal leakage and due to smaller supply pressure drop.

3. EXPANDER MODEL

The semi-empirical model of a scroll expander described hereunder is deduced from the one proposed by Winandy et al. [13] for hermetic scroll compressors. It is similar to the model of Kane [1], but describes internal and external heat transfers (and requires three additional parameters). The model has already been partially validated by tests with steam as working fluid (Lemort et al. [14]). In this paper, the model parameters are identified for the expander under investigation, integrated into a Rankine cycle and fed with HCFC-123.

The conceptual scheme of the expander model is shown in Figure 4. In this model, the evolution of the fluid through the expander is decomposed into the following consecutive steps:

a) Adiabatic supply pressure drop (su→ su,1),
b) Isobaric supply cooling-down (su,1 → su,2),
c) Adiabatic and reversible expansion to the "adapted" pressure imposed by the built-in volume ratio of the machine (su,2 → ad),
d) Adiabatic expansion at a constant machine volume (ad → ex,2),
e) Adiabatic mixing between supply and leakage flows (ex,2 → ex,1),
f) Isobaric exhaust cooling-down or heating-up (ex,1 → ex).

From the description given in Figure 4, it can be observed that the heat transfers, the supply pressure drop and the internal leakage are fictitiously dissociated from the actual expansion process (*su,2 → ex,2*). All the processes mentioned hereunder are described in the following paragraphs.

3.1. Supply pressure drop

The supply pressure drop ($P_{su} - P_{su,1}$) accounts for all pressure losses encountered by the fluid from the suction line to the suction chamber. Major pressure losses are associated to two following phenomena (Yanagisawa et al. [5]):

- As shown in Figure 5, during part of the suction process, the expander suction port is blocked by the tip of the orbiting scroll, reducing the effective suction port.
- At the end of the suction process, the flow passage between the central portion of the suction chamber and the two adjacent crescent-shaped portions is progressively reduced to zero. However, the tip seal does not extend to the end of the scrolls, which increases the flow between the central and the adjacent chambers and attenuates the supply pressure drop.

The lumped supply pressure drop is computed by comparison to the isentropic flow through a converging nozzle, whose cross sectional area A_{su} is a parameter to identify. Because of the steady-state nature of the model, this cross sectional area represents an average value of the suction port effective area over the entire suction process (that extends over one shaft revolution).

By combination of the equations of mass and energy conservation through the nozzle, the mass flow rate entering the expander can be expressed as:

$$\dot{M} = \frac{A_{su}}{v_{thr,su}} \sqrt{2\left(h_{su} - h_{su,1}\right)} \tag{4}$$

Both the specific enthalpy and the specific volume at the nozzle throat are function of the pressure $P_{su,1}$ at the throat and of the supply specific entropy s_{su}. Knowing the mass flow rate entering the expander, Eq. (4) can be used to compute the pressure $P_{su,1}$.

3.2. Supply and exhaust heat transfers

The main heat transfer mechanisms inside the scroll expander occur between: 1) the expander shell and the fluid in the supply and exhaust pipes; 2) the scrolls (fixed and orbiting) and the fluid in the suction, expansion and discharge chambers; 3) between the shell and the ambient.

Both supply and exhaust heat transfers are computed by introducing a fictitious metal envelope of uniform temperature T_w. This fictitious envelope represents the metal mass associated to the expander shell, the fixed and the orbiting scrolls. The supply heat transfer is given by:

$$\dot{Q}_{su} = \dot{M} \cdot \left(h_{su,1} - h_{su,2}\right) = \left[1 - e^{\left(\frac{-AU_{su}}{\dot{M}.c_p}\right)}\right] \cdot \dot{M} \cdot c_p \cdot \left(T_{su,1} - T_w\right) \tag{5}$$

The supply heat transfer coefficient AU_{su} is assumed to vary with the mass flow rate according to:

$$AU_{su} = AU_{su,n} \cdot \left(\frac{\dot{M}}{\dot{M}_n}\right)^{0.8} \tag{6}$$

where $AU_{su,n}$ is the nominal heat transfer coefficient corresponding to the nominal mass flow rate $\dot{M}_n$. This relationship can be justified by the Reynold's analogy for a turbulent flow through a pipe (Incropera and DeWitt [15]) by assuming that the fluid

properties, not included in this expression, remain unchanged. Exhaust heat transfer is described in a similar way.

3.3. Internal leakage

There are two different leakage paths in a scroll compressor/expander: the radial leakage is due to a gap between the bottom or the top plate and the scrolls and the flank leakage results from a gap between the flanks of the scrolls (Halm, [16]). In this modeling, all the leakage paths are lumped into one unique fictitious leakage clearance, whose cross-sectional area A_{leak} is a parameter to identify. The leakage flow rate can be computed by reference to the isentropic flow through a simply convergent nozzle, whose throat area is A_{leak}. The pressure at the inlet of the nozzle is $P_{su,2}$. The throat pressure corresponds to the maximum between exhaust and critical pressures:

$$P_{thr,leak} = MAX\left(P_{ex,2}, P_{crit,leak}\right) \tag{7}$$

The critical pressure $P_{crit,leak}$ is computed by considering the refrigerant vapor as a perfect gas:

$$P_{crit,leak} = P_{su,2}\left[\left(\frac{2}{\gamma+1}\right)^{\left(\frac{\gamma}{\gamma-1}\right)}\right] \tag{8}$$

As for the supply pressure drop, the mass and energy conservation equations through the nozzle are combined to express the leakage mass flow rate:

$$\dot{M}_{leak} = \frac{A_{leak}}{v_{thr,leak}} \sqrt{2\left(h_{su,2} - h_{thr,leak}\right)} \tag{9}$$

3.4. Displaced mass flow rate

As shown in Eq. (10), the internal mass flow rate $\dot{M}_{in}$ is the difference between the mass flow rate $\dot{M}$ entering the expander and the leakage mass flow rate $\dot{M}_{leak}$. The entering mass flow rate is the volume flow rate $\dot{V}_{s,exp}$ divided by the specific volume of the fluid $v_{su,2}$ after pressure drop and cooling down. The volume flow rate is the swept volume $V_{s,exp}$ multiplied by the expander rotational speed *N*. The swept volume in expander mode is equal to the one in compressor mode $V_{s,exp}$ divided by the built-in volume ratio of the machine $r_{v,in}$.

$$\dot{M}_{in} = \dot{M} - \dot{M}_{leak} = \frac{\dot{V}_{s,exp}}{v_{su,2}} - \dot{M}_{leak} = \frac{N.V_{s,exp}}{v_{su,2}} - \dot{M}_{leak} = \frac{N}{v_{su,2}}.\frac{V_{s,cp}}{r_{v,in}} - \dot{M}_{leak} \tag{10}$$

3.5. Internal expansion

One working cycle of the scroll expander includes three processes: suction, expansion and discharge (Halm, [16]). During the *suction* process, the suction chamber is in communication with the suction line and the fluid flows into the chamber. The *expansion* process is initiated when the suction chamber ceases to be in communication with the suction line. The *discharge* process begins when the discharge chambers enter in communication with the discharge line.

The internal power $\dot{W}_{in}$ produced by the machine is the summation of the suction ($\dot{W}_{suc}$), the expansion ($\dot{W}_{\text{expan}}$) and discharge ($\dot{W}_{dis}$) powers. Moreover, since the internal expansion process (*su,2* → *ex,2*) is assumed adiabatic, the internal power can be expressed as function of initial and final enthalpy states:

$$\dot{W}_{in} = \dot{W}_{suc} + \dot{W}_{\text{expan}} + \dot{W}_{dis} = \dot{M}_{in}(h_{su,2} - h_{ex,2}) \tag{11}$$

3.5.1. Suction power

The energy balance across the suction chamber, between the beginning and the end of the suction process yields:

$$\dot{W}_{suc} = \dot{M}_{in}(h_{su,2} - u_{su,2}) = \dot{M}_{in} P_{su,2} v_{su,2} = P_{su,2} \dot{V}_{s,exp} \tag{12}$$

3.5.2. Expansion power

The expansion process is assumed to be adiabatic and reversible. Writing the energy balance between the beginning and the end of this process yields:

$$\dot{W}_{\text{expan}} = \dot{M}_{in}\left(h_{su2} - P_{su2} v_{su2} - h_{ad} + P_{ad} v_{ad}\right) \tag{13}$$

3.5.3. Under- and over-expansion

Under-expansion occurs when the internal pressure ratio imposed by the expander (P_{su2}/P_{ad}) is lower than the system pressure ratio (P_{su2}/P_{ex2}). In that case, the pressure in the expansion chambers at the end of the expansion process (P_{ad}) is higher than the pressure in the discharge line. This is represented in Figure 6 (a). The modeling assumes that there is no pressure drop through the discharge port. In order to equalize the pressures in the discharge chambers (the former expansion chambers) and in the discharge line, some fluid ($\Delta\dot{M}_{in}$ in Eq. (14)) has to flow out of the discharge chambers. The modeling assumes it is achieved instantaneously as soon as the expansion chambers open onto the discharge line. The energy balance over the discharge chamber can be expressed as follows:

$$\left(\dot{M}_{in} - \Delta\dot{M}_{in}\right)u_{ex,2} - \dot{M}_{in}u_{ad} = -\Delta\dot{M}_{in}h_{ex,2} \tag{14}$$

Over-expansion occurs when the internal pressure ratio imposed by the expander is higher than the system pressure ratio (Figure 6 (b)). The energy balance over the discharge chamber is then similar to the one already established for the under-expansion process:

$$\left(\dot{M}_{in} + \Delta\dot{M}_{in}\right)u_{ex,2} - \dot{M}_{in}u_{ad} = \Delta\dot{M}_{in}h_{ex,2} \tag{15}$$

There is no work directly associated to the under- and over-expansion throttling.

3.5.4. Discharge power

As for the suction process, the equation of conservation of energy is applied on the discharge chamber between the beginning and the end of the discharge process, yielding:

$$\dot{W}_{dis} = -\left(\dot{M}_{in} \pm \Delta\dot{M}_{in}\right) P_{ex,2} v_{ex,2} = -r_{v,in} P_{ex,2} \dot{V}_{\mathrm{s,exp}} \tag{16}$$

3.5.5. Internal power

The internal power can be found by combining Equations (12), (13) and (16):

$$\dot{W}_{\mathrm{in}} = \dot{M}_{in}\left[\left(h_{su,2} - h_{ad}\right) + v_{ad}\left(P_{ad} - P_{ex,2}\right)\right] \tag{17}$$

3.6. Shaft power

Mechanical losses $\dot{W}_{\mathrm{loss}}$ are due to friction between the scrolls and losses in the bearings. In the present modeling, all these losses are lumped into one unique mechanical loss torque T_{loss}, that is a parameter to identify. The modeling assumes that this torque is independent of the rotational speed (Yanagisawa et al. [5]). Accordingly, the expander shaft power can be defined by:

$$\dot{W}_{sh} = \dot{W}_{in} - \dot{W}_{loss} = \dot{W}_{in} - \dot{W}_{loss} = \dot{W}_{in} - 2.\pi.N_{rot}.T_{loss} \tag{18}$$

3.7. Heat balance over the expander

The ambient losses are computed by introducing a global heat transfer coefficient AU_{amb} between the envelope and the ambient:

$$\dot{Q}_{amb} = AU_{amb}(T_w - T_{amb}) \tag{19}$$

Mechanical losses are directly "injected" into the envelope. In steady-state regime, the envelope temperature is computed by expressing its energy balance:

$$\dot{W}_{loss} - \dot{Q}_{ex} + \dot{Q}_{su} - \dot{Q}_{amb} = 0 \tag{20}$$

4. VALIDATION OF THE EXPANDER MODEL

The validation of the expander model is achieved in two steps. First, the values of the parameters of the model are identified on the basis of the measurements. Then, predictions by the model are compared to measurements. Relative deviations are then used to determine the quality of fit.

4.1. Identification of the parameters of the model

The parameter identification process is illustrated in the flow chart given in Figure 7. The input variables of the model are the supply pressure, the supply temperature, the exhaust pressure and the rotational speed of the expander. The model calculates the

mass flow rate displaced by the expander, the delivered mechanical power and the exhaust temperature. The model only necessitates eight parameters, which are summarized in Table 3. The nominal mass flow rate $\dot{M}_n$ is only introduced as a reference to define the nominal heat transfer coefficients $AU_{su,n}$ and $AU_{ex,n}$. Imposing the supply pressure as an input variable and the mass flow rate as an output variable is purely a convention. In fact, the mass flow rate could be imposed as an input (in the experimental set-up, it is actually imposed by the pump) and the supply pressure would be predicted by the model.

The parameters of the model are identified by minimizing a global error function accounting for the errors on the prediction of the mass flow rate, shaft power and exhaust temperature (which are the main output variables of the model):

$$error = \frac{1}{3}\left(\sqrt{\sum_{1}^{N_{tests}}\left(\frac{\dot{M}_{calc}-\dot{M}_{meas}}{\dot{M}_{calc}}\right)^2}\right)+\frac{1}{3}\left(\sqrt{\sum_{1}^{N_{tests}}\left(\frac{\dot{W}_{sh,calc}-\dot{W}_{sh,meas}}{\dot{W}_{sh,calc}}\right)^2}\right)+\frac{1}{3}\left(\sqrt{\sum_{1}^{N_{tests}}\left(\frac{T_{ex,calc}-T_{ex,meas}}{T_{ex,meas,max}-T_{ex,meas,min}}\right)^2}\right) \quad (21)$$

This minimization process is carried out by means of a genetic algorithm available in the EES software (Klein [12]). The identified parameters are listed in Table 3.

4.2. Validation of the model

Figure 8 compares the evolutions of the mass flow rate measured and predicted by the model with the expander supply specific volume, for the three different rotational speeds. The mass flow rate decreases with the specific volume of the refrigerant and

increases with the rotational speed. It can be observed that the agreement between the measurement and the prediction by the model is very good. The maximum deviation is 2%.

The evolutions of the shaft power, measured and predicted by the model, with the pressure ratio are compared in Figure 9. Here also, it can be observed that the agreement is good. The maximum deviation between the model predictions and the measurements is 5%.

Figure 10 compares the evolutions of the exhaust temperature (measured and predicted by the model) with the mean measured temperature of the fluid between the expander supply and exhaust.

The model predicts the exhaust temperature within 3 K. However, the model seems to slightly overestimate the exhaust temperature for high expander mean temperatures and to slightly underestimate it for the lower mean temperatures.

This figure also shows the evolution of the predicted exhaust temperature if the model did not account for ambient losses. The deviation between the predicted exhaust temperature and the measured one increases with the mean temperature. This confirms that the model should account for the ambient losses to better predict the exhaust temperature.

5. MODEL ANALYSIS

The validated model of the expander is used to quantify the different losses and to indicate how the design of the expander might be altered to achieve better performances.

Figure 11 shows the evolution of the overall isentropic effectiveness with the pressure ratio imposed to the expander. Operating conditions, related to one of the measured performance points, correspond to a supply pressure of 10.03 bar, an exhaust pressure of 2.01 bar, a supply temperature of 142°C and a rotational speed of 2296 rpm. The measured overall isentropic effectiveness for this operating point is also indicated in Figure 11 (with error bars associated with measurement uncertainties).

The evolution at the top of the figure is predicted by a model that only accounts for under- and over-expansion losses. The effectiveness goes through 1.0 at a pressure ratio equal to the internal pressure ratio (P_{ad}=P_{ex}). For smaller and larger pressure ratios, the fluid is over-expanded and under-expanded respectively. Experimental results showed that the maximum achieved pressure ratio was around 5.5. If much larger pressure ratios were imposed, a machine with a larger built-in volume ratio than 4.05 would yield better performances.

The overall isentropic effectiveness decreases when accounting for the heat transfers in the modeling because of the supply cooling down of the fluid. This decrease could

slightly be tempered by better insulating the expander (in the limiting case, $AU_{amb}=0$ W/K).

Introducing the mechanical losses and the supply pressure drop in the modeling largely reduces the isentropic effectiveness. Further work should investigate the possibility of reducing mechanical losses by using better adapted tip seals. As already mentioned by Yanagisawa et al. (2001), the supply pressure drop is an inherent characteristic of the scroll machine. A detailed modeling of the expander should answer the question of how to reduce this pressure drop by modifying the expander geometry.

The internal leakage is responsible for the major part of the performance loss. Under the assumption that the tip seals work correctly (they seal the radial gap between the tip of each scroll and the plate of the opposite scroll), the identified leakage area (Table 3) may be explained by a large flank clearance between the two scrolls. This large clearance is characteristic of scroll machines operating with a kinematically rigid configuration, where a flank gap is maintained.

6. CONCLUSIONS

An experimental study was carried out on a prototype of a scroll expander integrated into an Organic Rankine Cycle. The evolution of the expander performance, expressed in terms of global isentropic effectiveness and filling factor, with the operating

conditions has been investigated. The tested prototype achieved a maximum isentropic effectiveness of 68%.

Based on experimental results, the eight parameters of a semi-empirical simulation model of the expander have been identified. The model, with its parameters identified, predicts the mass flow rate, the shaft power and the exhaust temperature with a good accuracy.

The validated model of the expander was used to quantify the different losses and to indicate how the design of the expander might be altered to achieve better performances. This analysis pointed out that the internal leakages and, to a lesser extent, the supply pressure drop and the mechanical losses are the main losses affecting the performance of the expander.

Due to its accuracy, low computational time and robustness, the model can easily be integrated into a Rankine cycle simulation model. The variation of the performance of the cycle with the performance of the expander could therefore be investigated. The model could also be used as a pre-design tool for estimating the main characteristics of the expander.

7. REFERENCES

[1] M. Kane, D. Larrain, D. Favrat, Y. Allani, Small hybrid solar power system, Energy 28 (2003) 1427-1443.

[2] S. Quoilin, Experimental study and modeling of a low temperature Rankine Cycle for small scale cogeneration, Master thesis, Université de Liège, Belgium, 2007.

[3] J.-G. Persson, Performance mapping vs design parameters for screw compressors and other displacement compressor types, VDI Berichte, nr. 859, Düsseldorf, 1990.

[4] R. Zanelli, D. Favrat, Experimental Investigation of a Hermetic Scroll Expander-Generator, in: Proceedings of the International Compressor Engineering Conference at Purdue, 1994, 459-464.

[5] T. Yanagisawa, M. Fukuta, Y. Ogi, T. Hikichi, Performance of an oil-free scroll-type air expander, in: Proceedings of the ImechE Conference on Compressors and their Systems, 2001, 167-174.

[6] J. Manzagol, P. d'Harboullé, G. Claudet, G. Gistau Baguer, Cryogenic scroll expander for Claude cycle with cooling power of 10 to 100 watts at 4.2 K, Advances in Cryogenic Engineering, in: Proceedings of the Cryogenic Engineering Conference - CEC AIP Conference, 2002, 267-274.

[7] G. Xiaojun, L. Liansheng, Z. Yuanyang, S. Pengcheng, Research on a Scroll Expander Used for Recovering Work in a Fuel Cell, International Journal of Thermodynamics 7 (2004) 1-8.

[8] J. Hugenroth, J. Braun, E. Groll, G. King, Experimental investigation of a liquid-flooded Ericsson cycle cooler, International Journal of Refrigeration 31 (2008), 1241-1252.

[9] B. Aoun, D. Clodic, Theoretical and experimental study of an oil-free scroll type vapor expander, in: Proceedings of the Compressor Engineering Conference, Purdue, 2008, Paper 1188.

[10] R.B. Peterson, H. Wang, T. Herron, Performance of a small-scale regenerative Rankine power cycle employing a scroll expander, in: Proceedings of the IMechE Vol. 222 Part A: J. Power and Energy, 271-282.

[11] T. Inaba, M. Sugihara, T. Nakamura, T. Kimura, E. Morishita, A scroll compressor with sealing means and low pressure side shell, in: Proceedings of the International Compressor Engineering Conference, Purdue, USA, 1986, 887-900.

[12] S.A. Klein, Engineering Equation Solver, F-Chart Software, Middleton, WI, 2008.

[13] E. Winandy, C. Saavedra, J. Lebrun, Experimental analysis and simplified modelling of a hermetic scroll refrigeration compressor, Applied Thermal Engineering 22 (2002) 107-120.

[14] V. Lemort, I. V. Teodorese, J. Lebrun, Experimental Study of the Integration of a Scroll Expander Into a Heat Recovery Rankine Cycle, in: Proceedings of the International Compressor Engineering Conference, Purdue, 2006, C105.

[15] F. P. Incropera, D. P. DeWitt, Fundamentals of Heat and Mass Transfer, John Wiley & Sons, 2002.

[16] N. P. Halm, Mathematical Modeling of Scroll Compressors, Master Thesis, Purdue University, West Lafayette, IN, 1997.

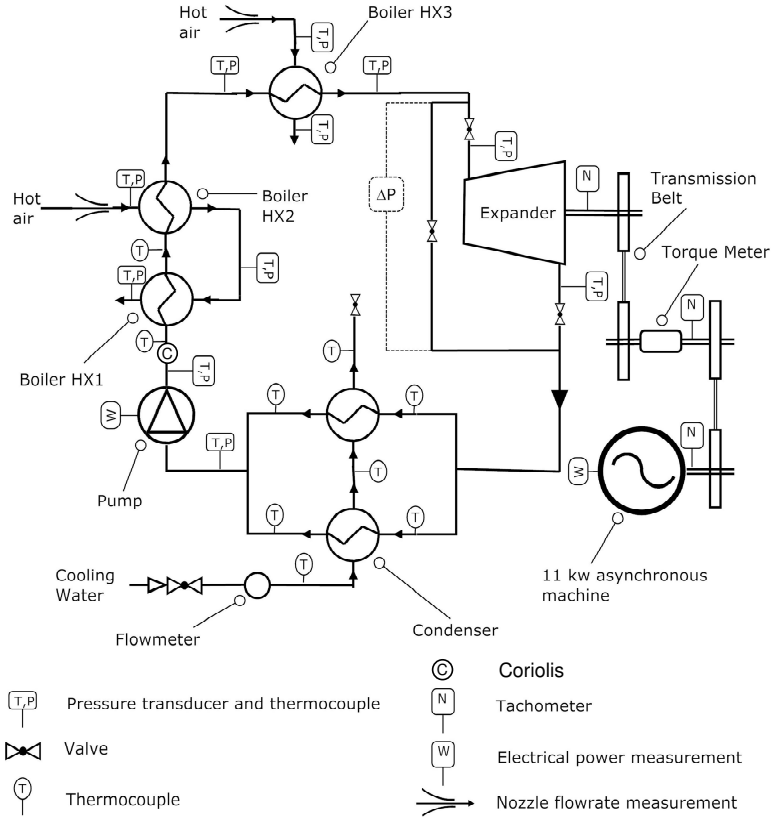

Figure 1: Schematic representation of the ORC test bench

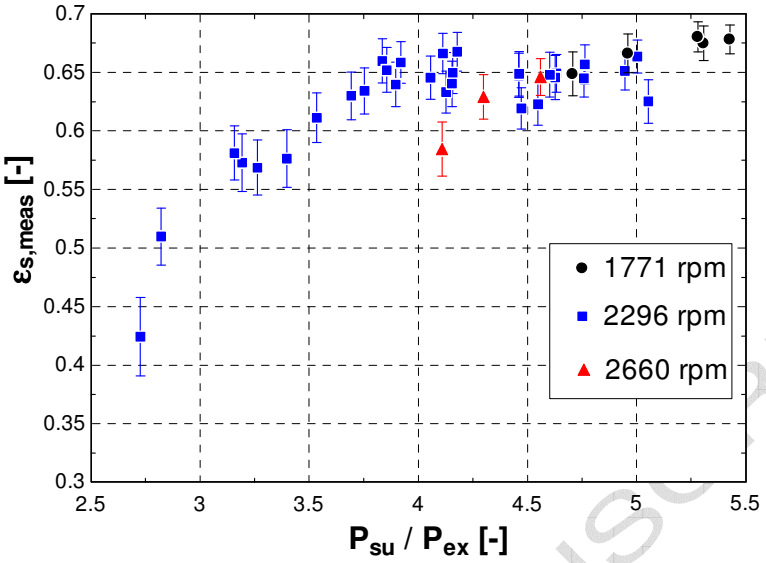

Figure 2: Evolution of the measured expander overall isentropic effectiveness with the imposed pressure ratio

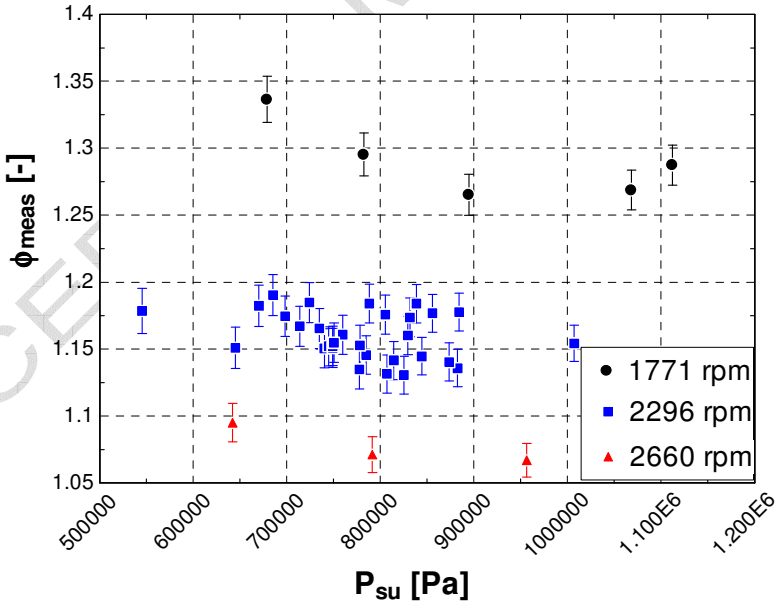

Figure 3: Evolution of the measured filling factor with the supply pressure

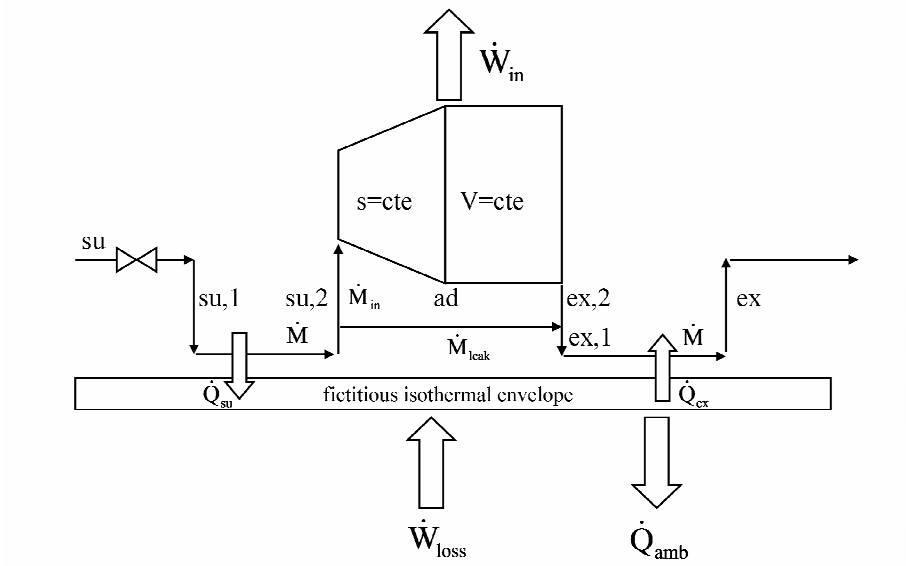

Figure 4: Conceptual scheme of the expander model

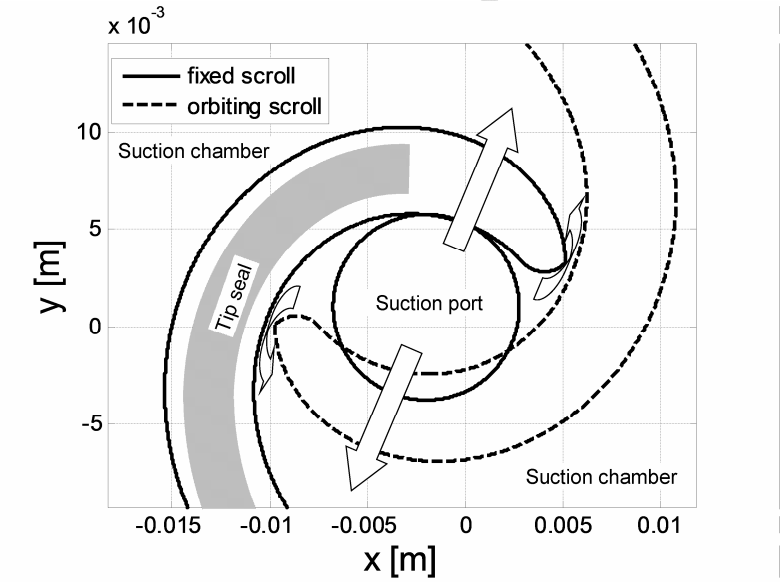

Figure 5: Representation of the suction chambers at the end of the suction process

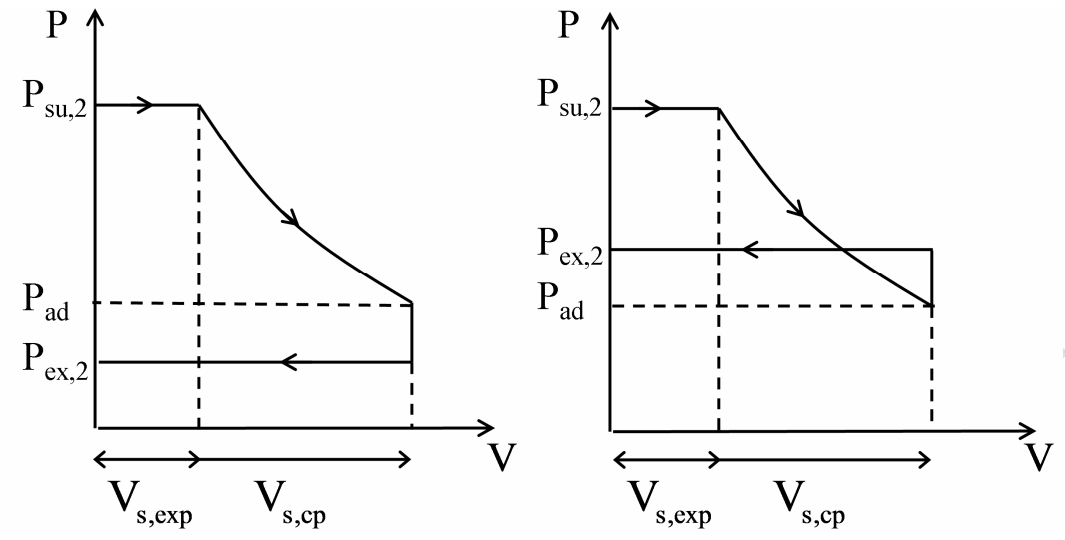

(a) **(b)**

Figure 6: Representation of the entire expansion process in the pressure-volume diagram ((a): under-expansion and (b): over-expansion)

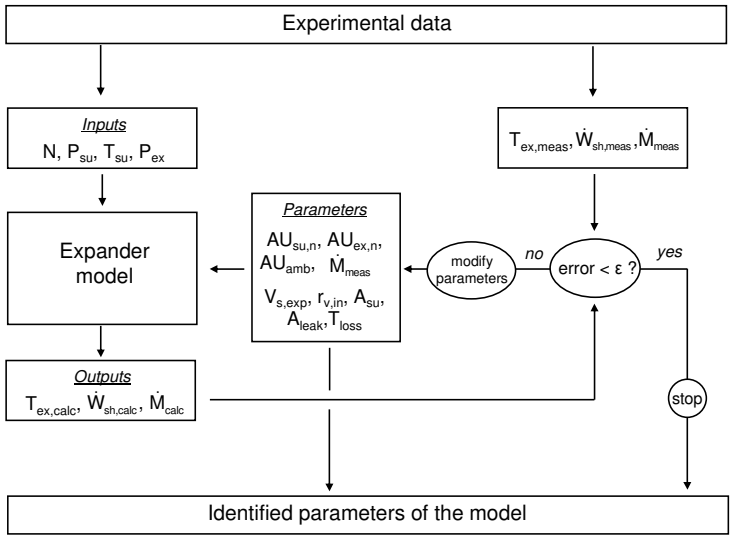

Figure 7: Flow chart of the parameter identification process

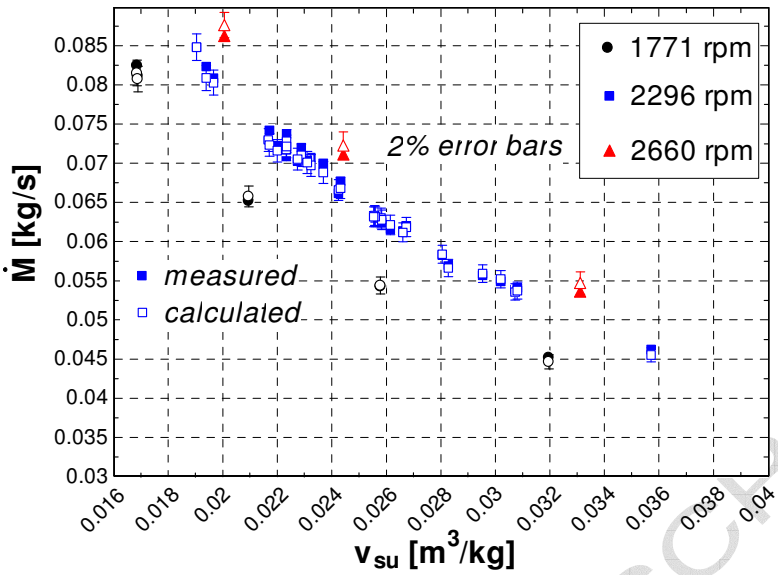

Figure 8: Evolution of the mass flow rate (predicted and measured) with the specific volume at the expander supply

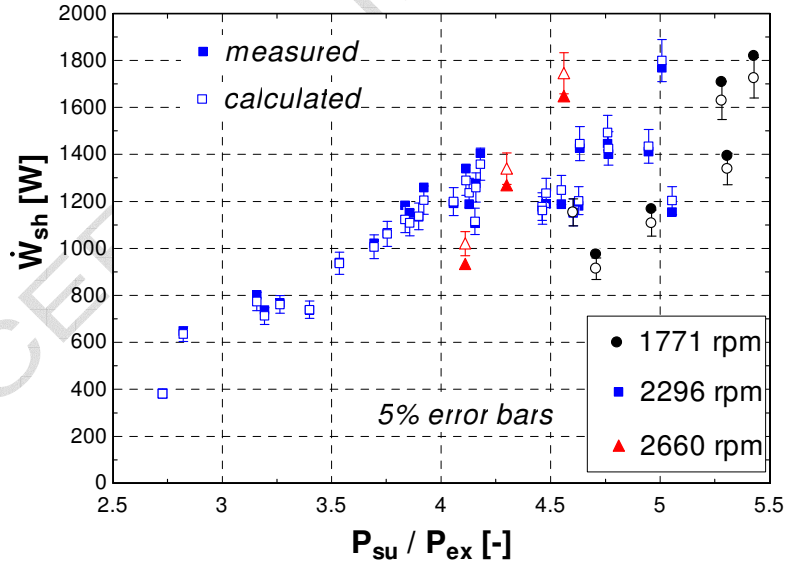

Figure 9: Evolution of the expander shaft power (measured and predicted by the model) with the imposed pressure ratio

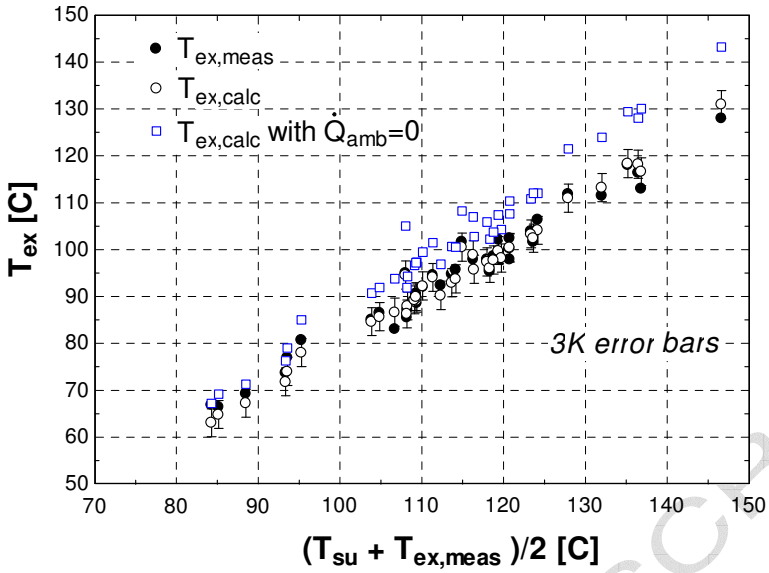

Figure 10: Evolution of the exhaust temperature (measured and predicted by the model) with the mean fluid temperature between the expander supply and exhaust

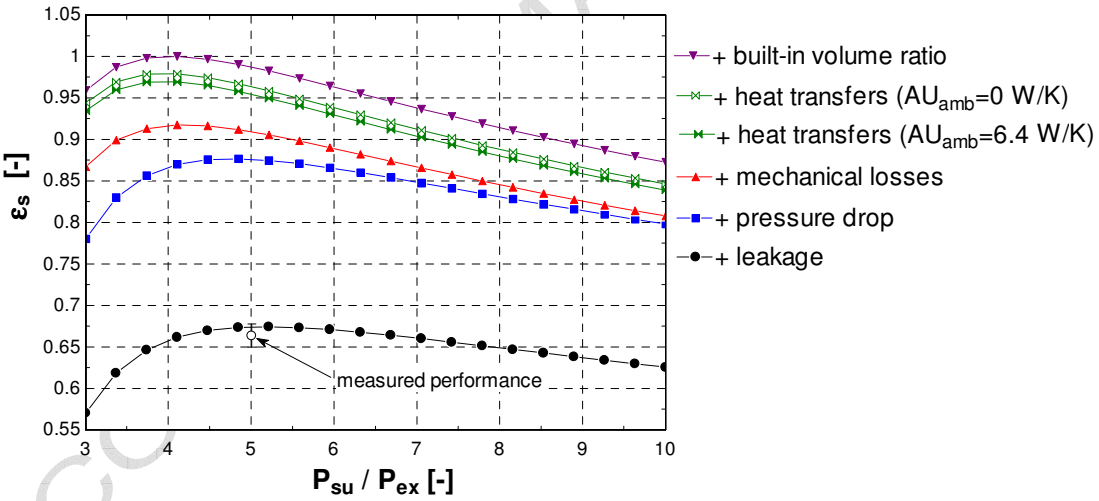

Figure 11: Evolution of the calculated overall isentropic effectiveness with the imposed pressure ratio

Table 1: Accuracy of the measurement devices

Variable		Device uncertainty
Torque	T_{tqm}	± 0.1 N.m
Temperature	T	± 0.3 K
Supply pressure	P_{su}	± 0.05 bar
Exhaust pressure	P_{ex}	± 0.025 bar
Mass flow rate	$\dot{M}_{meas}$	± 0.1%

Table 2: Ranges of the main measured variables

Imposed					*Obtained*				
$\dot{M}_{meas}$	$T_{su,meas}$	$\Delta T_{su,meas}$	$P_{ex,meas}$	N	$\dot{W}_{sh,meas}$	$P_{su,meas}$	$T_{ex,meas}$	$\varepsilon_{s,meas}$	φ_{meas}
[g/s]	[°C]	[K]	[bar]	[min^{-1}]	[W]	[bar]	[°C]	[-]	[-]
45.13 – 86.25	101.7 – 165.2	2.2 – 68.9	1.38 – 2.66	1771 – 2660	382 – 1820	5.45 – 11.12	66.4 – 128.0	0.424 – 0.680	1.067 – 1.336

Table 3: Identified parameters of the expander model

Heat transfer coefficient with the ambient	AU_{amb}	6.4 W/K
Supply heat transfer coefficient	$AU_{su,n}$	21.2 W/K
Exhaust heat transfer coefficient	$AU_{ex,n}$	34.2 W/K
Nominal mass flow rate	$\dot{M}_n$	0.12 kg/s
Leakage area	A_{leak}	4.6 mm^2

Built-in volume ratio	$r_{v,in}$	4.05
Swept volume	$V_{s,exp}$	36.54 cm^3
Supply port cross-sectional area	A_{su}	27.43 mm^2
Mechanical loss torque	T_{loss}	0.47 N.m